Groundwater

Hydrogeologic Controls on Induced Seismicity in Crystalline Basement Rocks Due to Fluid Injection into Basal Reservoirs

by Yipeng Zhang[1], Mark Person[2], John Rupp[3], Kevin Ellett[3], Michael A. Celia[4], Carl W. Gable[5], Brenda Bowen[6], James Evans[7], Karl Bandilla[4], Peter Mozley[1], Thomas Dewers[8], and Thomas Elliot[4]

Abstract

A series of M_b 3.8–5.5 induced seismic events in the midcontinent region, United States, resulted from injection of fluid either into a basal sedimentary reservoir with no underlying confining unit or directly into the underlying crystalline basement complex. The earthquakes probably occurred along faults that were likely critically stressed within the crystalline basement. These faults were located at a considerable distance (up to 10 km) from the injection wells and head increases at the hypocenters were likely relatively small (~70–150 m). We present a suite of simulations that use a simple hydrogeologic-geomechanical model to assess what hydrogeologic conditions promote or deter induced seismic events within the crystalline basement across the midcontinent. The presence of a confining unit beneath the injection reservoir horizon had the single largest effect in preventing induced seismicity within the underlying crystalline basement. For a crystalline basement having a permeability of 2×10^{-17} m^2 and specific storage coefficient of 10^{-7}/m, injection at a rate of 5455 m^3/d into the basal aquifer with no underlying basal seal over 10 years resulted in probable brittle failure to depths of about 0.6 km below the injection reservoir. Including a permeable ($k_z = 10^{-13}$ m^2) Precambrian normal fault, located 20 m from the injection well, increased the depth of the failure region below the reservoir to 3 km. For a large permeability contrast between a Precambrian thrust fault (10^{-12} m^2) and the surrounding crystalline basement (10^{-18} m^2), the failure region can extend laterally 10 km away from the injection well.

Introduction

The sixfold increase of earthquakes during the past decade in the midcontinent region of the United States (Ellsworth et al. 2012) has been attributed to deep injection of fluids (Frohlich 2012). This information has increased interest in reducing the risk of induced seismic events associated with unconventional oil/gas brine reinjection and from other deep waste disposal wells. Similar concerns have been raised regarding proposed future industrial-scale deployment of carbon-capture and storage projects across the midcontinent, particularly with regard to inducing fractures in overlying confining units (Zoback and Gorelick 2012). The issue of induced seismicity gained widespread attention following a series of relatively large earthquakes (up to M_b 5.5) that were associated with hazardous waste injection at the Rocky Mountain Arsenal, Colorado, in 1966 (Healy et al. 1968; Hsieh and Bredehoeft 1981) (Figure 1A) and through confirmation of the hydraulically induced failure mechanism in controlled experiments at Rangley Colorado (Raleigh et al. 1972, 1976). At the Rocky Mountain Arsenal near Denver, earthquakes occurred within the crystalline basement when the fluid pressures were raised over 320 m above hydrostatic conditions (3.2 MPa) between a depth of about 0.7–7 km (Hsieh and Bredehoeft 1981). The maximum wellhead injection pressure was measured at 7.6 MPa (Figure 1B). However, much lower pressure changes are thought to have been responsible for the M7.9 Wenchuan earthquake in Sichuan province, China that killed over 80,000 people (Kerr and Stone 2009). Ge et al. (2009) used hydromechanical modeling

[1]Department of Earth and Environmental Science, New Mexico Institute of Mining and Technology, 801 Leroy Place, Socorro, NM 87801.
[2]Corresponding author: Department of Earth and Environmental Science, New Mexico Institute of Mining and Technology, 801 Leroy Place, Socorro, NM 87801; (575) 835-6506; fax: (575) 835-6436; mperson@nmt.edu
[3]Indiana Geological Survey, Indiana University, 611 North Walnut Grove, Bloomington, IN 47405-2208.
[4]Department of Civil Engineering, Princeton University, E-208 E-Quad, Princeton, NJ 08544.
[5]Los Alamos National Laboratory, EES-16, Los Alamos, NM 87545.
[6]Department of Earth and Atmospheric Sciences, Purdue University, 550 Stadium Mall Drive, West Lafayette, IN 47907.
[7]Department of Geology, Utah State University, Logan, UT 84322-4505.
[8]Sandia National Laboratory, Albuquerque, NM.
Received November 2012, accepted April 2013.

doi: 10.1111/gwat.12071

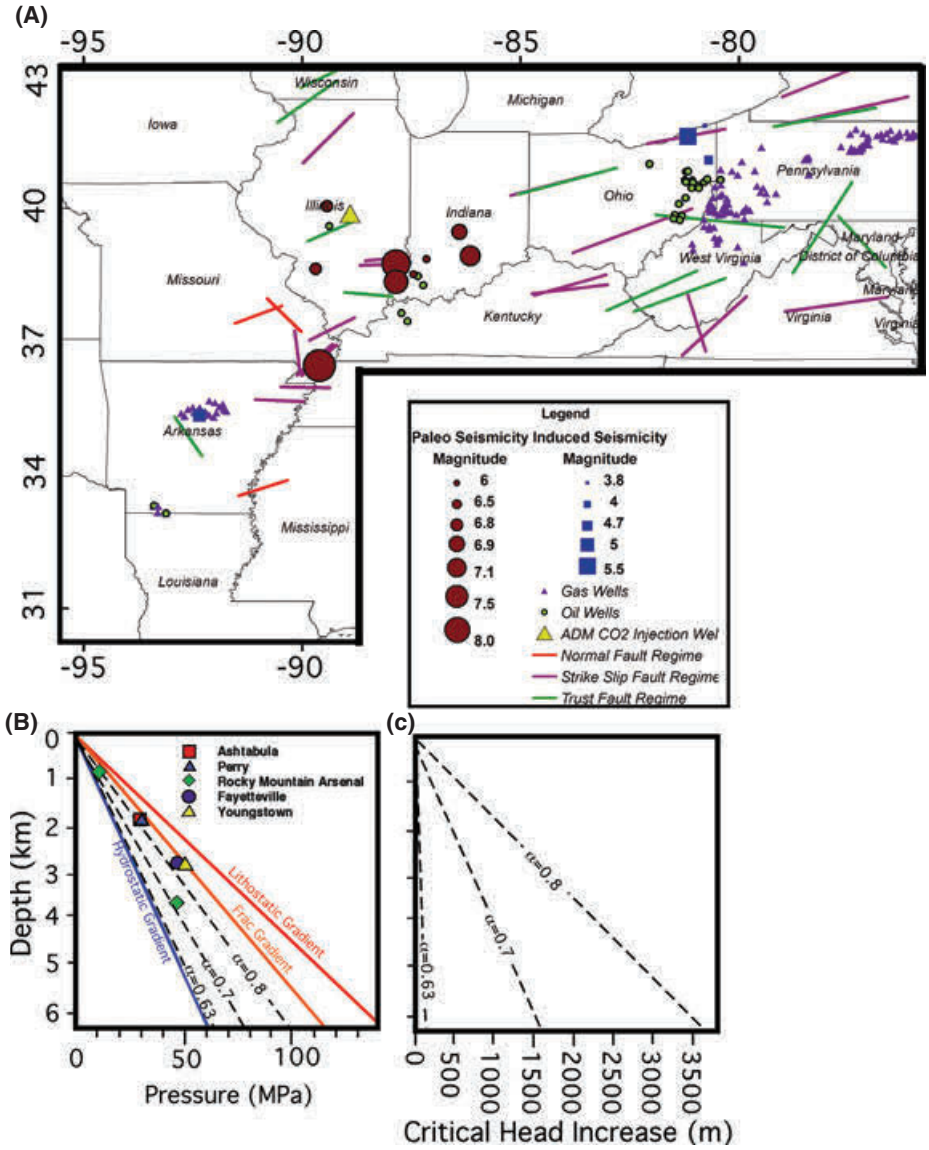

Figure 1. (A) Location and magnitude of induced earthquakes associated with hazardous waste injection (blue squares) as well as Holocene/Anthropocene earthquakes (red circles) for the midcontinent region, United States (modified from Wheeler and Cramer, 2002; Nicholson and Wesson, 1999; Horton et al. 2012). The magnitude of the earthquakes is proportional to the symbol size (see legend). Note that while many earthquakes occurred near the injection wells, only the largest induced seismic event is plotted. Lines indicate orientation of horizontal principal stress (σ_1; after Zoback and Zoback 1989; Heidbach et al. 2010). The density and locations of reinjection wells can be inferred from the distribution on current oil (green circles) and gas (blue triangles) wells (source: www.bakerhughes.com). The location of the CO_2 injection well near Decatur Illinois is shown by the yellow triangle. (B) Well-head injection pressure and injection depth for known sites having induced earthquakes (square, triangle, diamond, and circle symbols). The lithostatic pressure gradient (red line) denotes the vertical stress associated with the weight of the rock column (23 MPa/km). The hydrostatic pressure gradient (10 MPa/km) reflects static fluid pressure (blue line). The frac gradient is assumed to be 80% of the lithostatic pressure gradient (orange line). The dashed lines in (B) denote the critical pressures (see Equation 4) for three different values of α. (C) Plot of head increases required for failure for the three values of α plotted in (B).

to argue that the Wenchuan earthquake was caused by filling of the nearby Zipingpu dam ($\Delta h \sim 100$ m), located 5.5 km from the epicenter. Ge et al. (2009) estimated that filling of the dam only resulted in a head change of 2.5–5 m (0.025–0.05 MPa) at a depth of 10–20 km below the land surface near the earthquake foci. Saar and Manga (2003) also concluded that small head changes (about 1 m or 0.01 MPa) were required to induce earthquake swarms 4.5 km below Mt. Hood, Oregon. The head changes at depth were thought to be the result of propagation of near-surface, seasonal, 10 m water table fluctuations. Less is known about pore pressure changes associated with the recent earthquakes near Guy, Arkansas (Horton 2012) and Youngstown, Ohio, related to brine injection from unconventional energy development. Little information is available regarding the pressure conditions at the earthquake hypocenters, located up to 10 km away from the injection wells. Although most of the induced earthquakes

associated with hazardous waste injection have been relatively small ($<M_b$ 5), paleoseismic indicators, such as liquefaction features (e.g. sand dikes) from the midcontinent, suggest that parts of this region have experienced large, damaging earthquakes between M6 and M8 (Figure 1A) (Obermeier et al. 1992; Munson et al. 1997; Wheeler and Cramer 2002; Obermeier 2009). The mechanism for these large, historical, and Holocene seismic events within the stable interior of the craton is not well known; they may be due, in part, to the compression of low-permeability crystalline basement rocks in response to flexure of the crust that is associated with post-glacial rebound (Grollimund and Zoback 2000; Neuzil 2012).

The recent induced earthquakes (Figure 1A) are thought to be triggered by either hazardous waste injection wells or the reinjection of produced brines from unconventional gas development (see oil and gas wells depicted as green circles and purple triangles, respectively, in Figure 1A). The majority of these earthquakes did not occur within the sedimentary reservoirs where the fluids were injected, but rather 1–4 km deeper within the underlying crystalline basement (Nicholson and Wesson 1990; Seeber and Armbruster 1993; Seeber et al. 2004; Horton 2012). Two notable exceptions are the Rocky Mountain Arsenal (Healy et al. 1968; Hsieh and Bredehoeft 1981) and Youngstown, Ohio cases where the fluids were injected directly into the crystalline basement. Because no low-permeability, laterally extensive confining layers isolated the storage reservoir from the underlying crystalline basement in all of these instances, we hypothesize that elevated pore pressures could propagate downward along distributed fracture networks or along conductive fault zones in Precambrian crystalline rocks. Seismological and mechanical considerations require earthquakes that radiate energy to form at depth (<4 km) within the crystalline basement (Scholz 2002). Crystalline basement faults typically have higher coefficients of friction than sedimentary basin faults. In addition, the maximum principal stresses tend to increase with depth (Nicholson and Wesson 1990), and the overall stiffness of the cold midcontinent basement may result in larger stress drops when slip on faults does occur.

To date, environmental regulations concerning the greater than 150,000 oil and gas brine reinjection wells have focused on ensuring that pore pressures are kept below the fracture limit of 80% of lithostatic pressure (orange line, Figure 1B) and that brines do not migrate upward into shallow aquifers. Similar regulations are being implemented for large-scale carbon capture and storage (CCS) projects (USEPA 2010). Downward fluid pressure propagation, because of injection of dense brines or supercritical CO_2 into the crystalline basement, has not been considered from a regulatory perspective. One concern regarding the existing regulations is that fluid pressures associated with induced seismic events never reached the fracture limit of the reservoir rocks (symbols in Figure 1B) (Hsieh and Bredehoeft 1981; Nicholson and Wesson 1990; Seeber and Armbruster 1993; Zoback and Harjes 1997; Seeber et al. 2004). The pressures reported in Figure 1B were measured at the well head. Pressure changes at the earthquake hypocenters, located over 10 km away in some instances (Nicholson and Wesson 1990), must have been much lower. This suggests that many of the faults were critically stressed and required only a modest increase in pore pressure to cause slip (Barton et al. 1995; Townend and Zoback 2000; Zoback and Townend 2001).

The U.S. National Research Council report on induced seismicity by Hitzman et al. (2012) noted that one important research direction is identifying the most critical geological characteristics that could contribute to induced seismicity. A major goal of this study is to analyze the hydrogeologic conditions of midcontinent injection sites where induced seismicity is known to occur. We hypothesize that the presence of transmissive normal and reverse faults hosted within the crystalline basement can play an important role in transmitting pore pressure anomalies deep into the crystalline basement, increasing the risk of a seismic event. In this study, we use a simple analytic-numerical model to evaluate what hydrogeologic conditions and injection scenarios that might either promote or impede the rapid propagation of anomalous pore pressures downward into the crystalline basement. We present results from a suite of simulations in which we varied the permeability of the crystalline basement, reservoir, and confining units, as well as Precambrian and Paleozoic normal faults and Precambrian thrust faults, located at different distances from a hypothetical injection well. We also considered the effects of a Precambrian-thrust fault hosted within the crystalline basement about 2 km below the injection well. Perhaps most importantly, we considered injection into basal reservoirs with no bottom seal verses injection into mid-level reservoirs sandwiched between two confining units. One goal of these models was to try to reproduce the hydrogeologic conditions associated with induced seismic events across the midcontinent from Ohio to Arkansas.

Our analysis predicts regions of pore pressure increase within the crystalline basement below an injection well that are high enough to cause failure along critically stressed faults. Because the geometry and depth of the predicted failure envelope calculated in some of our models are qualitatively similar to known hypocenter locations near injection wells in the midcontinent region, one might conclude that our model is capable of predicting earthquakes at proposed injection sites with no known history of seismicity. However, it would be erroneous to assume this. The predicted failure envelopes presented below do not guarantee that an earthquake would occur at any given site. This is because there is no guarantee that a critically stressed fault actually exists within the failure region. The National Research Council's report on induced seismicity by Hitzman et al. (2012) notes that there are over 150,000 injection wells currently permitted in the United States and only few have resulted in "felt" induced seismic events. Given the number of injection wells drilled to date and the number of reported associated

induced seismic events, the probability is actually quite low that a felt earthquake would occur at any given site.

Because the focus of this study is the Midcontinent region, United States, where several induced earthquakes have occurred recently, our analysis considers hydrogeologic conditions within the Illinois Basin. The southern Illinois Basin hosts the Wabash Valley Seismic Zone, where paleoseismic indicators suggest that a number of large (M6–M7.9) earthquakes have occurred in the past 12,000 years (Figure 1A). The Illinois Basin hosts a thick sequence of laterally extensive Cambrian-Ordovician sheet sandstones and carbonates, along with three shale-rich confining units. Many of the strata found in the Illinois Basin exist across the Midcontinent region, although the formation names may change. The basal Mount Simon Sandstone is considered a primary target for geologic carbon sequestration in the Illinois Basin and throughout the Midwest region (Person et al. 2010). The first demonstration-scale, saline formation carbon capture, and storage project in the United States with injection of 1 million mt supercritical CO_2 over a 3-year period commenced in November, 2011, with injection into the Mount Simon Sandstone at Decatur, Illinois (see triangle, Figure 1A; http://www.fossil.energy.gov/news/techlines/2012/12056-Carbon_Storage_Partner_Completes_F.html). This formation is underlain by granitic rocks of the Precambrian crystalline basement complex (McBride et al. 2007).

The regional stress state in the midcontinent area is characterized primarily by strike-slip to reverse faulting (Figure 1A). Under these conditions, the vertical load represents the intermediate principal stress. The maximum horizontal stress is oriented northeast to east across the midcontinent (Figure 1A) (Zoback and Zoback 1989; Heidbach et al. 2010). A series of deep basement faults associated with historic and induced seismic events in this region have been identified by Seeber et al. (2004); McBride et al. (2007), and Horton (2012).

Methods

Transport Equations

The calculation of head or pore pressure changes and rock failure analysis associated with hazardous-waste injection, CCS, or engineered geothermal systems typically requires the use of computationally expensive, three-dimensional (Burbey 2006), multiphysics codes, such as FEHM (Kelkar et al. 2012) and TOUGH2-FLAC (Rutqvist et al. 2007). The calculations usually include close coupling between fluid flow, heat transfer, and geomechanics. If multiple fault zones are considered, these codes likely require implementation on high-performance computers. Following the approach of Celia and Nordbotten (2009), we have developed a hybrid analytical-numerical, cross-sectional model, which honors the linear feature of the fault zones, as well as the radial pressure change patterns associated with hazardous waste/supercritical CO_2 injection wells within reservoirs. In this study, we consider a single injection well. Because of the short time-scale (10 years) and the high pressure changes considered, we neglect variable-density fluid-flow effects that could be important on longer time-scales after injection has ceased.

The mathematical model for groundwater flow in fault zones, the Precambrian crystalline basement, and sedimentary rock layers (excluding the injection reservoir) is given by:

$$\frac{\partial}{\partial x}\left[K_x\frac{\partial h}{\partial x}\right]+\frac{\partial}{\partial z}\left[K_z\frac{\partial h}{\partial z}\right]=S_s\frac{\partial h}{\partial t} \tag{1}$$

where x and z are the horizontal and vertical coordinates, respectively, S_s is the specific storage, h is the hydraulic head, t is time, and K_x and K_z are hydraulic conductivities in the horizontal and vertical directions, respectively. Equation 1 represents single-phase flow in a two-dimensional, cross-sectional, Cartesian coordinate system. This coordinate system was chosen because faults are long-linear features that are not well represented in a radial coordinate system. In most instances, vertical flow dominates outside of the injection reservoir.

We used the analytical solution of Hantush (1960) to calculate deviatoric heads within the reservoir. Hydraulic head increases within a reservoir near a single injection well are characterized by radial flow. The governing groundwater flow equation solved by Hantush (1960) is given by:

$$\frac{1}{r}\frac{\partial s}{\partial r}+\frac{\partial^2 s}{\partial r^2}-\frac{K_1}{T}\frac{\partial s_1}{\partial z}-\frac{K_2}{T}\frac{\partial s_2}{\partial z}=\frac{S}{T}\frac{\partial s}{\partial t} \tag{2}$$

where T is transmissivity of the reservoir ($T=Kb$, where b is the thickness of the formation); s is the head change above hydrostatic conditions in the reservoir; K_1 and K_2 are the vertical hydraulic conductivities of the upper and lower confining units, respectively; s_1 and s_2 are the head changes in the upper and lower confining layers at the interface between the reservoir and the confining units, respectively; S is the storage coefficient ($S=S_s b$); and r is radial distance from the injection well. This solution permits leakage across semipermeable top and bottom confining units. In order to calculate leakage out of the reservoir, Hantush (1960) solved two vertical diffusion equations within the upper and lower confining units:

$$\begin{aligned}\frac{\partial^2 s_1}{\partial z^2}&=\frac{S'}{b_1 K_1}\frac{\partial s}{\partial t}\\ \frac{\partial^2 s_2}{\partial z^2}&=\frac{S''}{b_2 K_2}\frac{\partial s}{\partial t}\end{aligned} \tag{3}$$

where S_s' and S_s'' are the specific storage coefficients within the upper and lower confining units, respectively. Hantush (1960) found an analytical solution for Equations 2 and 3 subject to a specified hydrostatic head boundary condition above the upper confining unit and either a hydrostatic head or a no-flux boundary at the base of the lower confining layer (see Supporting Information).

Solution Schemes, Boundary, and Initial Conditions

We solved Equation 1 using the finite element method (Reddy 1984). We used the solutions to Equations 2 and 3 as specified value boundary conditions throughout the injection reservoir. In this way, the radial behavior of head change propagation is captured analytically, while the Cartesian behavior, including head change propagation along the faults and in the crystalline basement, is captured with the finite element solution. We set the time step of the finite element model to 1 d and ran the model for 3650 d (10 years). This covers the time lag between the onset of injection and the timing of induced earthquakes reported by Nicholson et al. (1988), Nicholson and Wesson (1990), and Seeber et al. (2004). The stratigraphic units are discretized by triangular elements in a Cartesian coordinate system; this preserves the linear feature of the fault zones. Faults tend to have anisotropic hydraulic properties because of the formation of fault gouge and damage zones in crystalline basement rock or lithified sediments (Caine et al. 1996) and clay and sand smearing in unlithified sediments (Bense and Person 2006). The normal fault zone was 2 m wide, and the thrust fault was 10 m wide. Two elements were used to represent the fault zone in an equivalent, porous medium representation. The vertical and horizontal permeabilities of the fault zones were varied. The model domain was discretized into 3381 nodes and 6528 triangular elements. Element size varied from 1 to 800 m laterally and 10 to 300 m vertically. We used a telescoping grid with mesh refinement in the vicinity of the fault zone and the crystalline basement-sedimentary pile interface. The confining units were more highly discretized to minimize numerical grid diffusion. By linking the radial and Cartesian coordinate systems, our hybrid analytical-numerical model was able to approximate hydrologic conditions in response to injection into domains that included faults in two-spatial dimensions, which normally requires three-dimensional analysis. Our model was benchmarked, in part, by reproducing pressure change conditions for a single-well injection within a reservoir underlain by a thick bedrock unit using MODFLOW and by reproducing published model results from TOUGH2 for a multilayer, reservoir-confining-unit system by Birkholzer et al. (2009). The model results from Birkholzer et al. (2009) consider supercritical CO_2 injection (see Supporting Information).

In solving Equation 1, the top boundary of the model domain was set to be hydrostatic ($h = 2800$ m). The bottom of the solution domain was set to be a no-flux boundary. Both sides of the solution domain were set to be no-flux boundaries. We monitored calculated pressure changes within formations adjacent to the injection reservoirs and vertical fluxes out of the injection reservoir to ensure that the assumptions of the Hantush analytical solutions were honored (see Supporting Information).

Failure Criteria

We used a simple failure criterion proposed by Nicholson and Wesson (1990) for critically stressed-cohesionless faults under a stress regime, where the vertical stress (σ_v) is of a similar magnitude to the maximum horizontal stress (σ_1) (Lucier et al. 2006). Assuming a friction coefficient of 0.6, the critical pore pressure for failure along a fault plane (P_{crit}) is given by (Nicholson and Wesson 1990):

$$P_{crit} = \frac{\sigma_v}{2}(3\alpha - 1) \quad (4)$$

where σ_v is the vertical stress and α is the ratio of the minimum to maximum principal horizontal stress (σ_3/σ_1) (Jaeger and Cook 1979). This approach assumes that the vertical load (here we assume 23 MPa/km) can approximate the maximum principal stress, both of which increase with depth (Mark and Gadde 2008). In our simulations, we used an α value of 0.63 that falls in the middle of the range of stress measurements for the midcontinent region, reported by Lucier et al. (2006). This value was selected because it produced a predicted failure region that is consistent with the distribution of earthquake hypocenters generated from induced historical seismic events discussed below. This critical pressure includes both hydrostatic pressure and any increase in pore pressure above hydrostatic conditions as a result of pumping. The effect of the ratio of the minimum to maximum principal horizontal stress on the predicted pore pressure increase needed to cause failure is illustrated in Figure 1B using three different values of α (dashed lines labeled $\alpha = 0.63$, 0.7, and 0.8). We have also plotted the equivalent head increases (in m) with depth in Figure 1C (dashed) for these three values of α. At 5 km depth, the head increase required to cause failure is equal to about 120 m, 1330, and 3060 m for an α value of 0.63, 0.7, and 0.8, respectively. The edge of the failure region is where the computed pore pressure equals P_{crit} (Equation 4). Critically stressed faults within the failure region would be predicted to likely fail. A similar pressure criterion is used in FEHM to predict fault-plane failure (Kelkar et al. 2012). Our approach permits rapid analysis of a wide range of hydrogeological and injection scenarios. The methods described here can be modified for different geological conditions and rock properties.

Hydrogeologic Framework Model

The midcontinent hydrogeologic framework model used in this study is based on stratigraphic (Figure 2A) and permeability data (see boxplot, Figure 3) from the Illinois Basin. The Illinois Basin is characterized by a Paleozoic sedimentary pile containing a series of siliciclastic and carbonate reservoirs, separated by three major confining units (Eau Claire Formation, Maquoketa Shale, and New Albany Shale). Precambrian normal (Figure 2C) and thrust (Figure 2E) faults have been identified by seismic studies (McBride et al. 2007) and inferred by earthquake swarms (Nicholson and Wesson 1990; Horton 2012) that are thought to be associated with natural and induced seismic events. Some of the normal faults cut the lower units of the sedimentary pile (Figure 2D), although displacements are small and not represented here. Cambrian-Ordovician sandstone and carbonate reservoirs were the focus of this

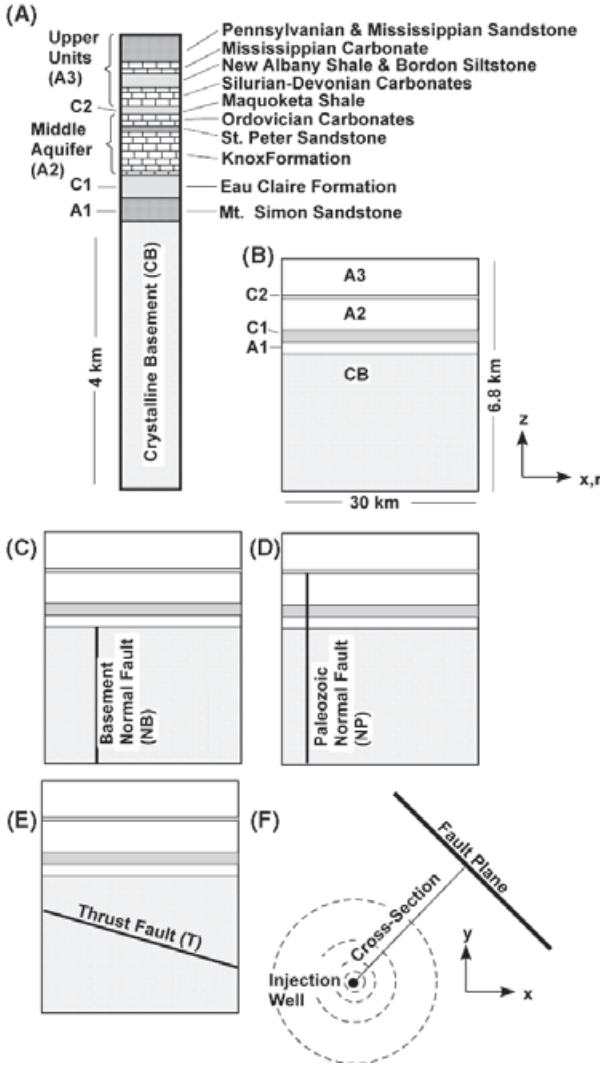

Figure 2. (A) Stratigraphic column representative of hydrogeologic conditions within the central Illinois Basin. In order to simplify our graphical presentation of model results, we lump many of the thin middle and upper lithologic units together into the reservoirs labeled A2 and A3 (B). Each layer was included in our finite element model calculations (Table 1). Note that C1 and C2 denote shale confining layers and A1 to A3 denote sandstone and carbonate reservoirs. For middle reservoir injection we used the average hydraulic conductivities of the middle reservoir units in the Hantush (1960) analytical solution. Injection was into A1 and A2. In some model scenarios, we included a Precambrian normal fault within the crystalline basement (C), a Paleozoic normal fault (D) which terminated within the middle reservoir (A2), and a low angle, Precambrian thrust fault (E) with a dipping angle of 30°. Panel (F) presents a plan view schematic diagram showing position of the injection well, radial deviatoric head/pressure contours (dashed lines), and the position of a normal fault plane.

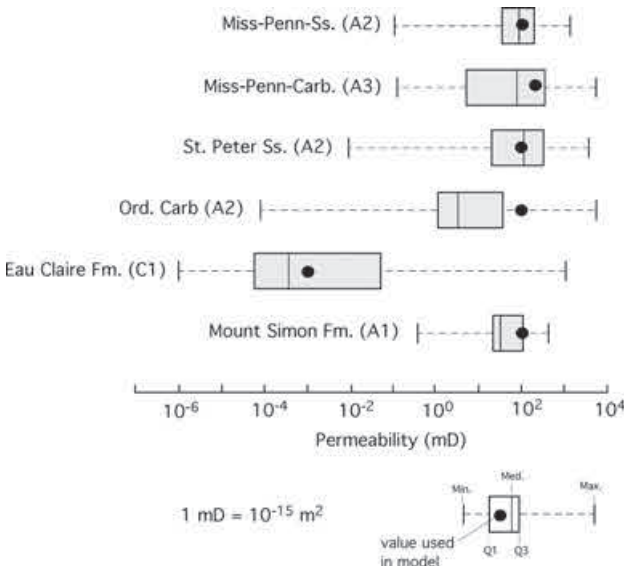

Figure 3. Boxplot of core permeability (in mD) for select formations within the Illinois Basin making up regional reservoirs (A1-A3) and confining unit (C1). The formations associated with different reservoirs or confining units are listed to the left of each boxplot. Black dots denote values used in this study. Abbreviations: A1, Aquifer 1; C1, contining unit 1; A2, aquifer 2 unit; Min., minimum permeability; Max., maximum permeability; Med., median permeability; Q1, 1st quartile; Q3, 3rd quartile; mD, millidarcy; Ord., Ordovician; Penn., Pennsylvanian; Miss., Mississippian; Carb., carbonate rock; S_s, sandstone.

study because of their high capacity of storage and suitable depth (>800 m) to store large quantities of supercritical CO_2 (Bandilla et al. 2012). Within this reservoir system, the Mount Simon Sandstone was assumed to be the primary injection reservoir, but we also considered Ordovician reservoirs (Knox Formation dolomites and St. Peter Sandstone) to be alternative injection units. The Mount Simon Sandstone is overlain by a top seal–the Eau Claire Formation–and is underlain by the crystalline basement. The Knox-St. Peter-Ordovician Carbonates reservoir units are overlain by the Maquoketa Shale (C2) and underlain by the Eau Claire Shale (C1), as shown in Figure 2A. The Precambrian crystalline basement is designated as CB in Figure 2B.

The solution domain used in this study extends laterally for 30 km from the injection point. Our model includes 2.8 km of sedimentary units underlain by 4 km of crystalline basement (CB, Figure 2B). Because our study is intended to apply to the midcontinent region, United States, we used typical permeabilities and strata thicknesses consistent with the Illinois Basin (Table 1, Figure 3). We considered injection of fluids into the basal Mount Simon Sandstone (A1, Figure 2B). This formation is capped by the Eau Claire Formation (C1, Figure 2B). For clarity of graphical presentation, and for our analytical calculations described above (Equation 2), we grouped a series of permeable Ordovician units, including the Knox Formation, St. Peter Sandstone, and upper-Ordovician Carbonates as the middle reservoir (A2, Figure 2B). These units are capped by the Maquoketa Shale confining unit (C2, Figure 2B). All other units above C2 are lumped into an upper reservoir (A3). It is important to note that all layers displayed in Figure 2A were represented in our numerical model.

We considered a range of permeabilities for the crystalline basement, as well as for normal and thrust faults

Table 1
Fixed hydrologic Properties Assigned to Midcontinent Hydrogeologic Model of Induced Seismicity

Formation Name	B (m)	k (m^2)	K (m/s)	S_s (1/m)	T (m^2/s)	Hydrostrat. Unit
Penn. Ss.	300	10^{-13}	10^{-6}	10^{-6}	3×10^{-4}	A3
Miss. Ss.	100	10^{-13}	10^{-6}	10^{-6}	10^{-4}	A3
Miss. Carb.	150	2×10^{-13}		10^{-6}	3×10^{-4}	A3
New Albany Sh.	200	10^{-18}	10^{-11}	3×10^{-6}	na	A3
Bordon Slt.	50	10^{-18}	10^{-11}	3×10^{-6}	na	A3
Sil.-Dev. Carb.	250	6×10^{-13}	6×10^{-6}	10^{-6}	1.5×10^{-3}	A3
Maq. Sh.	150	10^{-18}	10^{-11}	3×10^{-6}	na	C2
Ord. Carb.	150	10^{-13}	10^{-6}	10^{-6}	1.5×10^{-4}	A2
St. Peter Ss.	100	10^{-13}	10^{-6}	10^{-6}	10^{-4}	A2
Knox	550	10^{-13}	10^{-6}	10^{-6}	5.5×10^{-4}	A2
Eau Claire Sh.	400	10^{-18}	10^{-11}	3×10^{-6}	na	C1
Mt. Simon Ss.	400	10^{-13}	10^{-6}	10^{-6}	4×10^{-4}	A1
Crystalline Basement	4000	2×10^{-17}	2×10^{-10}	10^{-7}	na	CB

Abbreviations: CB, crystalline basement; A, aquifer; C, confining unit; na, not applicable; Ss., sandstone; Slt., Siltstone; Sh., shale; Carb., carbonate; Dev, Devonian; Sil, Silurian; Miss., Mississippian; Penn., Pennsylvanian; Maq., Maquoketa; B, formation thickness; k, permeability; K, hydraulic conductivity; S_s, formation specific storage; T, reservoir transmissivity.

(Table 2), in our sensitivity study. The normal faults were assumed to be hosted either in the Precambrian crystalline basement (NB) or lower-cut Paleozoic sedimentary units (NP). The throw on the normal faults was assumed to be negligible (Seeber et al. 2004; McBride et al. 2007). We only focused on the conduit effect of the fault, as represented in our model and did not explicitly represent the unmapped, critically stressed faults in the basement. Fixed hydrogeologic properties for the sandstone, carbonate, and shale units used in our model are listed in Table 1. In all model runs, the head changes are in response to 10 years of continuous injection at a rate of 5455 m^3/d (1000 gallons/min).

Petrophysical properties used in this study (black dots, Figure 3) were based on core permeability data (1 mD = 10^{-15} m^2). Within the Illinois Basin, permeability generally decreases with depth and porosity. However, there is a large variation in permeability (several orders of magnitude) that could be a result of pore size variations or diagenetic effects. The minimum and maximum permeability has a range of more than 4–7 orders of magnitude for most units. We typically chose effective permeability values higher than the median. Black dots are consistent with best fit values based on a model calibration exercise (not shown) that found regional salinity and stable isotope patterns (Zhang et al. 2011). We varied fault and crystalline basement permeability in our model runs (Table 2). The choice of bedrock permeability (3×10^{-16} to 10^{-18} m^2) falls within the range of variation of published permeability data (Manning and Ingebritsen 1999).

Results

Injection into Middle and Basal Reservoir

Modeling results indicate that after 10 years of continuous injection into the basal Mount Simon reservoir, the propagation of head changes above hydrostatic level and the failure region (orange pattern encompassing a

Table 2
Permeability (in m^2) Values Varied in Sensitivity Study

Model Run	Fault Type	Dist. Well-Normal Fault (m)	Fault Perm. (k_x, k_z)	Injection Reservoir	Basement Perm. ($k_x = k_y$)	Figure
1	—	—	—	A1	2×10^{-17}	4A
2	—	—	—	A2	2×10^{-17}	4B
3	NB	25	10^{-15}, 10^{-13}	A1	2×10^{-17}	4C
4	NB	5000	10^{-15}, 10^{-13}	A1	2×10^{-17}	4D
5	NP	25		A2	2×10^{-17}	4E
6	NP	5000		A2	2×10^{-17}	4F
7	—	—	—	A1	3×10^{-16}	5A
8	T	—	10^{-12}, 10^{-12}	A1	3×10^{-16}	5B
9	T, NB	500	10^{-12}, 10^{-12}	A1	10^{-18}	5C

Abbreviations: Perm., permeability; NB, normal fault hosted in Precambrian crystalline basement; NP, Paleozoic-normal fault cutting sedimentary units; A1; and C1; T, thrust fault.

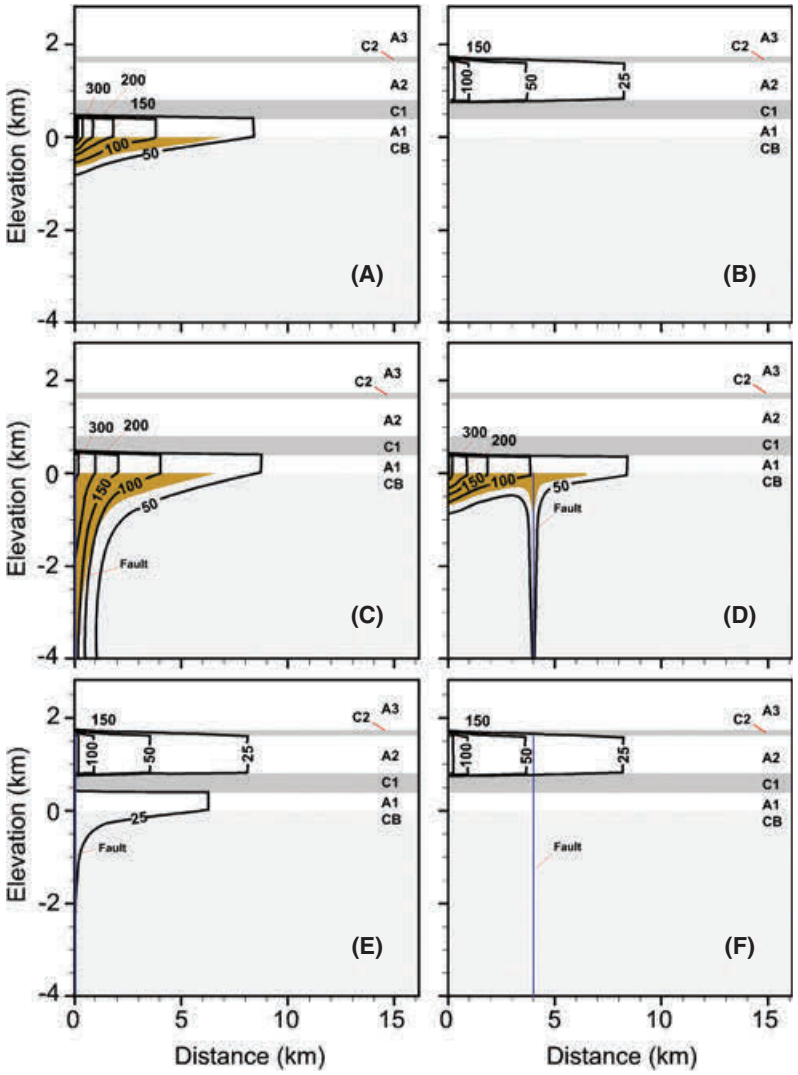

Figure 4. Computed changes in hydraulic head above hydrostatic conditions (in m) after 10 years of continuous injection at 5455 m^3/d within the basal (A) and middle (B) reservoir injection. No conductive faults are present in (A) and (B). A head of 100 m corresponds to pressure increase of 1 MPa above hydrostatic conditions. Changes in head for basal reservoir (A1) injection including a Precambrian normal fault located at 25 m and 4000 m from the injection well are presented in (C) and (D), respectively. The thin blue line denotes the location of the normal faults. The normal faults are 2 m wide. Panels (E) and (F) presented computed head changes for middle reservoir (A2) injection with Paleozoic normal fault located 25 m and 4000 m from the injection well, respectively. The Paleozoic normal fault cuts crystalline basement (C1), the basal Mount Simon Sandstone reservoir (A1), and the Eau Claire Formation. (C1). See Tables 1 and 2 for hydrogeologic parameters used in these simulations. The orange pattern denotes areas in the crystalline basement where computed total pressures (hydrostatic plus deviatoric pressures) are greater than the critical pressure computed using Equation 4. If a critically stressed fault is present in the area depicted by the orange pattern, then failure could occur.

region of heads between about 70 and 150 m) extended 600 m downward into the crystalline basement beneath the injection well (Figure 4A). The failure region penetration depth into the bedrock decreased away from the injection well to a distance of about 7 km. Because of the lower assigned permeability (10^{-18} m^2) and higher compressibility (3×10^{-6}/m) of the failure region compared to the crystalline basement (Table 1), head changes did not propogate far into the Eau Claire Shale. Injection into the middle aquifer (A2, Figure 4B) produced similar (though not identical) maximum deviatoric head and lateral head propagation when compared to the basal reservoir (Figure 4B). However, because the middle reservoir had a bottom seal (C1), elevated heads did not penetrate into the crystalline basement.

Effect of Conductive Vertical Basement Faults

For injection into the Mount Simon Sandstone (A1), including a permeable (10^{-13} m^2) Precambrian basement fault located 25 m from the injection well (Figure 4C) allowed head increases to penetrate to the base of the crystalline basement (4 km, Figure 4C). The pressure change envelope propagated laterally out of the fault plane about 500 m into the crystalline basement. If the conductive fault is located 4000 m from the injection well (Figure 4D), head increases and the failure region extend

down the fault zone 1000 m into the crystalline basement (Figure 4D). These increased heads are relatively small (between 60 and 160 m), yet could produce failure along a critically stressed fault for the value of α used (0.63). If a Paleozoic fault extends through the basal reservoir (A1) and the bottom seal (Eau Claire Formation confining unit, C2) at a distance of 25 m from the well and injection is into the middle reservoir (A2), then increased heads propagate down along the Paleozoic fault through the Eau Claire Formation into the Mount Simon Sandstone and the Precambrian basement (Figure 4E). However, the head increases were too low (~25 m) to produce a region of failure. When the conductive Paleozoic fault is located 4000 m from the well under the middle reservoir injection scenario, the region of increased heads and the failure region do not extend into the crystalline basement (Figure 4F).

Effect of Conductive Thrust Fault

We concluded our analysis by considering the effects of a conductive subhorizontal thrust fault. When a thrust fault is 300 times more permeable than the crystalline basement (Figure 5B), the 25 m head contour extends out about 1.5 km further (compare Figure 5A and 5B). The depth of penetration of head changes and the failure region is shallower for this scenario when compared with Figure 4A. Including the thrust fault in Figure 5B does not increase the lateral extent of the failure region. Although the basement permeability is higher (3×10^{-16} m^2) in Figure 5A and 5B than in previous models (2×10^{-17} m^2), these values are realistic (Manning and Ingebritsen 1999). If we had assigned a lower permeability crystalline basement (e.g. 10^{-18} m^2), then the pressure changes would not have reached the thrust fault beneath the well after 10 years of injection. If we add a highly conductive (10^{-12} m^2) normal fault at a distance of 500 m from the well and reduce the crystalline basement permeability to 10^{-18} m^2, then the envelope of head increases propagate laterally along the thrust fault plane a distance of 12 km (Figure 5C). The region of potential failure extends out along the fault about 10 km.

Discussion and Conclusions

The patterns of the failure region in Figures 4D and 5C qualitatively match the earthquake distribution reported in Northeastern Ohio (Nicholson et al. 1988) (Figure 6C and 6D) and Central Arkansas (Horton 2012) (Figure 6A and 6B). For Lake, Ohio, the depth of induced seismic events is greater beneath the injection well and shallows as one moves 5 km away from the region of highest pressure changes. A previously unmapped, conductive vertical fault at a distance of about 10 km from the injection well helped to promote seismic activity at depths (up to 4 km) within the crystalline basement. The head reaching the fault plane and triggering an earthquake in our model (Figure 4D) was about 90 m or 0.9 MPa, which exceeds the critical pore pressure (0.67 MPa) for this depth within the basal sandstone reservoir of the midcontinent region. Our thrust fault scenario with the connection to the high-permeability normal fault in Figure 5C reproduces the same features of observed seismicity data in central Arkansas (Figure 6A and 6B). Here, the Enders Fault, a subvertical normal fault cutting both the Ozark Aquifer and the Guy-Greenbrier thrust fault, provided a hydraulic connection to the injection well (Horton 2012). The lateral distance of the earthquake hypocenters from injection well #5 (Figure 6A) is about 10 km, which is about the same order of magnitude as the 12 km propagation distance of the failure region (Figure 5C). Our model results also suggest that the permeability difference between the Guy-Greenbrier thrust fault and the Precambrian basement must be about six orders of magnitude to allow the deviatoric pore pressures to propagate such a long distance. This lateral propagation distance also could have been accommodated by a wider fault zone with a lower permeability. It is important to note that our results depend on both the permeability, specific storage, and the α values

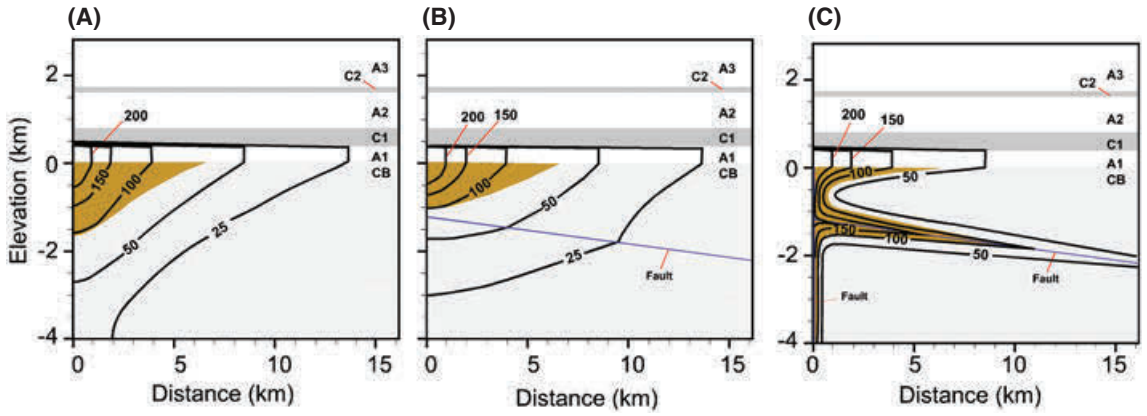

Figure 5. Computed changes in hydraulic head (m) above hydrostatic conditions after 10 years of continuous Mount Simon injection. In (A) and (B), the crystalline basement rock is relatively permeable (10^{-15} m^2) but no fault is present. In (B), a permeable thrust fault (10^{-12} m^2) is present in the crystalline basement. Panel (C) considers relatively low permeability basement (10^{-18} m^2) that hosts a permeable (10^{-12} m^2) thrust as well as a normal fault located 25 m from the injection well. See Tables 1 and 2 for hydrogeologic parameters used in these simulations. The thrust fault is 10 m wide.

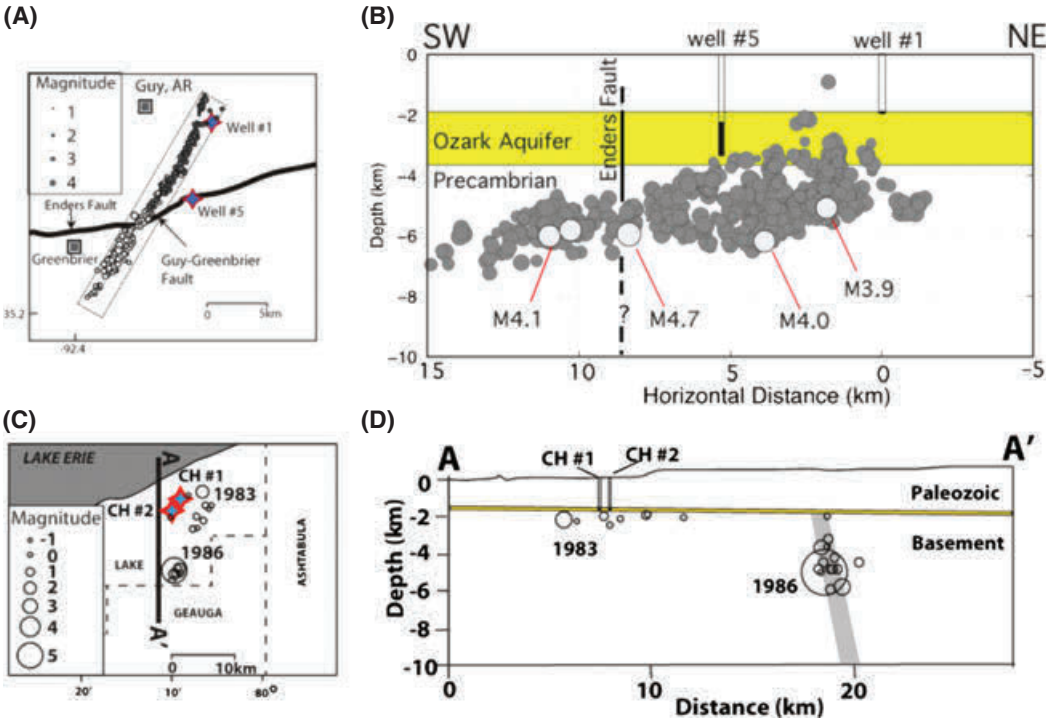

Figure 6. (A) Plan view map showing the location of two hazardous waste injection wells (stars) and earthquake epicenters near Guy Arkansas. Dark gray circles are earthquakes that occurred between October 1, 2010 and February 15, 2011. White circles are earthquakes that occurred between February 16, 2011 and March 8, 2011. Red and blue stars indicate locations of wells. (B) Cross section showing earthquake hypocenters looking N 60°W. The earthquake swarm is 3.2 km wide and dips 11° and is believed to represent the position of the Guy-Greenbrier fault zone. Yellow layer indicates the approximate vertical extent of the Ozark Aquifer. Solid black portion of each injection well indicates the interval where fluid is injected. The dashed line indicating the Enders fault is approximate. The larger earthquakes (light gray circles) rupture the deeper portions of the fault (after Horton 2012). (C) Plan view map showing locations of injection wells and earthquake epicenters 1983–1986 in Lake County, Ohio. Large uncertainties in location are associated with 1983 earthquake epicenters. (D) Cross section showing locations of induced earthquake hypocenters (circles) for Lake, Ohio. Circle size scales with earthquake magnitude (after Nicholson and Wesson 1990).

assigned. For example, had we used a value of 0.7 in the model, a failure envelope would not have formed in the crystalline basement without significantly increasing the injection rate or reducing the reservoir permeability.

The failure envelopes calculated using our model indicates where failure would occur if a critically stressed fault was present. As noted in the *Introduction*, the probability that a critically stressed fault being present within the failure envelop is quite low at any given location. However, in seismically prone regions that have experienced large, damaging earthquakes in the past (Figure 7), even a low-probability event needs to be taken seriously. We propose that injection into reservoirs with basal seals represents one strategy that could reduce the risk of induced seismic events. In the midcontinent region, there are several regional seals and mid-level carbonate reservoirs, such as the Knox formation (Figure 2A), that could serve as injection horizons.

Zhou et al. (2010); Person et al. (2010), and Bandilla et al. (2012) considered the hydrologic consequences of injecting large volumes of supercritical CO_2 into the basal Mt. Simon reservoir from distributed sources. These studies predicted that pressurization across the southern Illinois Basin would occur with regions of overlapping envelopes of increased pressure from adjacent injection sites. Bandilla et al. (2012) indicated that pressure change interference patterns in excess of 5 MPa are predicted to result from injection at numerous CO_2 injection sites across the southern Illinois Basin (colored contours, Figure 7). This region of excess pressure overlaps with the Wabash Valley Seismic Zone. Obermeier (2009) has outlined paleo-liquifaction features with similar ages (red-dashed lines in Figure 7) in the southern Illinois Basin. These areas may have experienced significant ground acceleration from damaging earthquakes (>M6) that are thought to have occurred during the last 12,000 years. Obermeier (2009) notes that the M 5.8 historical earthquakes near Vincennes, Indiana failed to produce sand dikes. This implies that the paleo sand dikes must have been formed from larger tremblers. Two studies have tried to estimate the magnitude of paleo-earthquakes that resulted in the paleoliquefaction features near Vincennes, Indiana with estimates that range between M7.2 and M7.5 (Green and Terri 2005; Olson et al. 2005).

Can additional measures be taken to reduce the risk of placing an injection well in an earthquake-prone, midcontinent region? In addition to our findings of including a basal seal, other important considerations

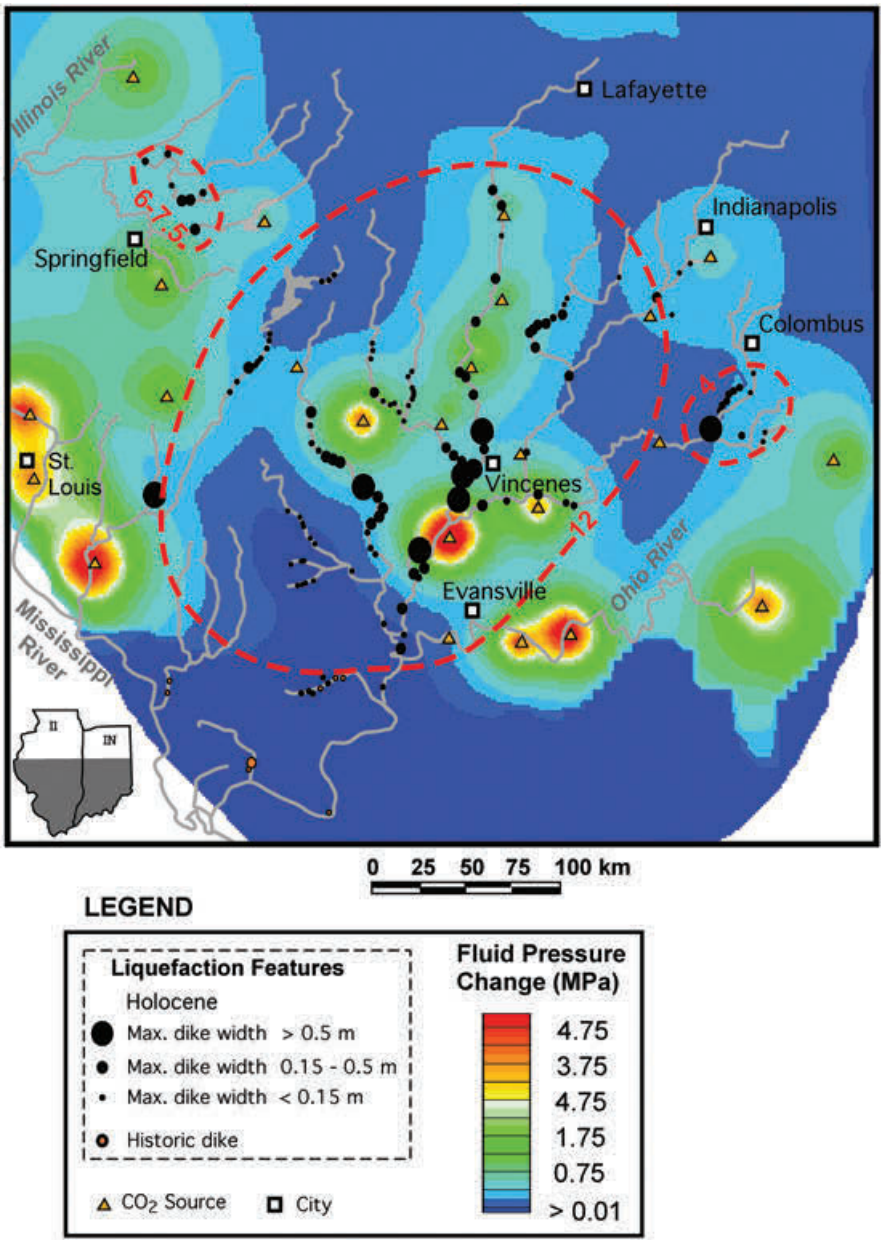

Figure 7. Map of southern Illinois Basin showing locations of paleo-liquifaction features (black circles) along stream-river network across. Liquefaction features from historic earthquakes are shown suing the orange circles. The size of the circles is proportional to the width of the sand dike (after Obermeier 2009). The red dashed lines group liquifaction features of similar age. The colored contours denote predicted increases in pressure due to proposed basin-scale CO_2 injection from distributed sources (orange triangles) across the southern Illinois Basin within the basal Mt. Simon reservoir. Predicted pore pressures due to proposed CO_2 injection are from Bandilla et al. (2012).

could include locating fault zones within the Precambrian crystalline basement rocks using seismic reflection data (e.g. McBride et al. 2007) and using available rock core data to identify indicators of the presence and hydraulic properties of nearby faults within Paleozoic strata in the vicinity of injection wells, such as deformation bands (e.g. Antonellini and Aydin 1995; Fossen et al. 2007; Chentnik and Bowen 2012). Basal reservoirs determined to be at risk of induced seismicity for CCS injection may need brine extraction strategies employed (e.g. Court et al. 2012) in order to control pressure buildup and propagation.

Nicholson and Wesson (1990) noted that as the orientation of the stress field moves away from the critically stressed, the value of α increases significantly and much higher pore pressures are needed to cause failure. We chose a value of α to be consistent with observed hypocenter depths and locations within the bedrock (Figure 6B and 6D). The large range of α values reported for the midcontinent region by Lucier et al. (2006), range between about 0.43 and 0.88, makes it impractical to apply our results to any given location. Site-specific modeling that accounts for in situ hydraulic properties of the host rock, pre-existing faults in the area, and the state of

stress at the locality would be needed to make any meaningful predictions of the potential for induced seismicity at a given location. Important insights might be gained from post-audit studies of induced seismic events using three-dimensional, geomechanical-hydrologic models.

Using the hydrologic (Table 1) and mechanical ($\alpha = 0.63$) parameters reported above, we found that failure was induced when computed hydraulic heads were about 70–150 m (0.7–1.5 MPa) above hydrostatic levels at a depth of 1–4 km below the reservoir-crystalline bedrock interface. Changes in pressure in our model were greater than those reported by Ge et al. (2009) and Saar and Manga (2003) but less than those reported for the Rocky Mountain Arsenal (Hsieh and Bredehoeft 1981; 320 m).

We have shown that the presence of a basal seal has a potentially important effect on reducing pressure increases in the crystalline basement, decreasing the risk of an induced seismic event. While many field sites in the midcontinent support our hypothesis, we are aware of two possible exceptions to this rule in the Western United States. Since 1991, the Bureau of Reclamation has been injecting shallow, naturally occurring brines within Paradox Valley in western Colorado that would otherwise flow into the Colorado River (Ake et al. 2005; O'Connell and Creed 2013). A series of shallow salinity abatement pumping wells collected the brine and injected it into the Leadville Limestone 4.3 km below land surface. Injection fluid pressures reached 82 MPa and induced up to 4000 earthquakes up to 3 km from the wellhead. The largest induced earthquake was M 4.3. The Leadville Limestone is underlain by Devonian and Cambrian strata. However, these authors indicate that the deep injection well was intentionally sited to intersect a highly fractured region of this formation in order to optimize fluid injection rates. The well intersected the Wray Mesa fault system that has acted as one of the principal zones of seismicity.

Meremonte et al. (2001) reported a close spatial correlation between the locations of a series of brine reinjection wells associated with coal bed methane production and the 2001 earthquake swarm (M3.4–M4.6) near Trinidad, CO. This same region experienced a M5.3 earthquake on August 23, 2011, the largest earthquake in Colorado since 1967. The seismic events were thought to have occurred within the crystalline basement in close proximity to where brines were injected into the Dakota Sandstone. The Dakota Sandstone is a midlevel reservoir at a depth of about 1.2 km. The Dakota is underlain by Pennsylvanian- and Permian-age Magdalena Groups and Sangre de Cristo Groups that contain shale units. The base of the sedimentary units is about 1.8 km. The earthquake swarm occurred at a depth of between 3 and 6 km within crystalline bedrock. Given the stratigrapahy underlying the Dakota, we hypothesize that a transmissive fault must have facilitated fluid transmission into the deep subsurface. We note that both of these counterexamples are in more tectonically active regions of the United States.

In summary, our study has shown that the majority of the midcontinent induced seismic events are associated with basal reservoir injection in which no bottom seal was present. The presence of conductive faults within the Precambrian crystalline basement played a critical role in allowing increased pore pressures to propagate downward. Our numerical model results suggest that injecting into a reservoir with both a bottom and top seal reduces the potential risk of induced seismicity. Such a strategy should be considered in areas that have experienced large seismic events in the past.

Acknowledgment

The authors gratefully acknowledge Paul Hsieh for his thorough review of this manuscript and thoughtful comments. Carl Gable and Mark Person thank the DOE IGGP program for their support of this research. Tom Dewers was supported as part of the Center for Frontiers of Subsurface Energy Security, an Energy Frontier Research Center funded by the U.S. Department of Energy, Office of Science, Basic Energy Sciences under Award Number DE-SC0001114. Sandia National Laboratories is a multi-program laboratory managed and operated by Sandia Corporation, a wholly owned subsidiary of Lockheed Martin Corporation, for the U.S. Department of Energy's National Nuclear Security Administration under contract DE-AC04-94AL85000.

Supporting Information

Additional Supporting Information may be found in the online version of this article:

Appendix S1. Discussion of Hantush analytic solution, model benchmark exercises, and verification of Hantush analytical solution assumptions

Figure S1. Plot of Hantush (1960) well function $H(u,\beta)$ verses $1/u$. The numbers on each line represent different values of β.

Figure S2. (A) Schematic diagram illustrating MODFLOW benchmark model domain geometry. The blue region schematically denotes the area of elevated pore pressures that are plotted in cross section in (B). (B) Comparison of computed head increases using MODFOW (solid black line) and our analytical-numerical model (red dashed lines) results assuming constant pumping for 10 years. The parameters used in the model are listed in Table S1.

Figure S3. (A) Cross-sectional schematic diagram showing geometry of reservoirs and confining units in a radial coordinate system with injection into the basal reservoir at $r = 0$ m. Comparison of published computed (excess) fluid pressures above hydrostatic conditions using TOUGH2 (solid black lines) and our hybrid analytical-numerical model (red dashed lines) due to fluid injection. Confining unit permeability was between 10^{-17} m^2 (B), 10^{-18} m^2 (C), 10^{-19} m^2 (D), and 10^{-20} m^2 (E). Results are after

30 years of continuous injection (after Birkholzer et al. 2009).

Table S1. Parameters used in MODFLOW benchmark study.

Table S2. Parameters used in TOUGH2 benchmark exercise.

References

Ake, J., K. Mahrer, D. O'Connell, and L. Block. 2005. Deep-injection and closely monitored induced seismicity at Paradox Valley, Colorado. *Bulletin of the Seismological Society of America* 95, no. 2: 664–683.

Antonellini, M., and A. Aydin. 1995. Effect of faulting on fluid flow in porous sandstones: Geometry and spatial distribution. *American Association of Petroleum Geologists Bulletin* 79: 642–671.

Bandilla, K.W., M.A. Celia, T.R. Elliot, M. Person, K.M. Ellett, J.A. Rupp, C. Gable, and Y. Zhang. 2012. Modeling carbon sequestration in the Illinois Basin using a vertically-integrated approach. *Computing and Visualization in Science*. In press.

Barton, C.A., M.D. Zoback, and D. Moos. 1995. Fluid flow along potentially active faults in crystalline rock. *Geology* 23: 683–686.

Bense, V.F., and M.A. Person. 2006. Faults as conduit-barrier system to fluid flow in silicilastic sedimentary aquifers. *Water Resources Research* 42, no. 5: 1–18.

Birkholzer, J.T., Q. Zhou, and C.-F. Tsang. 2009. Large-scale impact of CO_2 storage in deep saline aquifers: a sensitivity study on pressure response in stratified systems. *International Journal of Greenhouse Gas Control* 3: 181–194.

Burbey, T. 2006. Three-dimensional deformation and strain induced by municipal pumping, part 2:382 numerical analysis. *Journal of Hydrology* 330, no. 3–4: 422–434.

Caine, J.S., J.P. Evans, and C.B. Forster. 1996. Fault zone architecture and permeability structure. *Geology* 24, no. 11: 1025–1028.

Celia, M., and J.M. Nordbotten. 2009. Practical modeling approaches for geological storage of carbon dioxide. *Ground Water* 47, no. 5: 627–638.

Chentnik, B.M., and B.B. Bowen. 2012. Characterizing fractures and deformation bands. *Journal of Purdue Undergraduate Research* 2: 8–15.

Court, B., K.W. Bandilla, M.A. Celia, T.A. Buscheck, J.M. Nordbotten, M. Dobossy, and A. Janzen. 2012. Initial evaluation of advantageous synergies associated with simultaneous brine production and CO_2 geological sequestration. *International Journal of Greenhouse Gas Control* 8: 90–100.

Ellsworth, W.L., S.H. Hickman, A.L. Lleons, A. Mcgarr, A.J. Michael, and J.L. Rubinstein. 2012. Are seismicity rate changes in the midcontinent natural or manmade? (Abstract). *Seismological Society of America Annual Meeting* 83, no. 12: 137.

Fossen, H., R.A. Schultz, Z.K. Shipton, and K. Mair. 2007. Deformation bands in sandstone: A review. *Journal of the Geological Society of London* 164: 1–15.

Frohlich, C. 2012. Two-year survey comparing earthquake activity and injection-well locations in the Barnett Shale, Texas. *Proceedings of the National Academy of Sciences* 109, no. 35: 13934–13938. DOI:10.1073/pnas.1207728109.

Ge, S., M. Liu, N. Lu, J. Godt, and G. Luo. 2009. Did the Zipingpu Reservoir trigger the 2008 Wenchuan earthquake? *Geophysical Research Letters* 36, no. 20: 1–5. DOI:10.1029/2009GL040349.

Green, R., and G. Terri. 2005. Number of equivalent cycles concept for liquefaction evaluations—Revisited. *Journal of Geotechnical and Geoenvironmental Engineering* 131, no. 4: 477–488.

Grollimund, B., and M.D. Zoback. 2000. Post glacial lithospheric flexure and induced stresses and pore pressure changes in the northen North Sea. *Tectonophysics* 327: 61–81.

Hantush, M.S. 1960. Modification of the theory of leaky aquifers. *Journal of Geophysical Research* 65, no. 11: 3713–3732.

Healy, J.H., W.W. Rubey, D.T. Griggs, and C.B. Raleigh. 1968. The Denver earthquakes. *Science* 161, no. 3848: 1301–1310.

Heidbach, O., M. Tingay, A. Barth, J. Reinecker, D. Kurfeß, and B. Muüller. 2010. Global crustal stress pattern based on the World Stress Map database release 2008. *Tectonophysics* 482, no. 2010: 3–15.

Hitzman, M.W., D.D. Clarke, E. Detournay, J.H. Deiterich, D.K. Dillon, S.J. Green, R.M. Habiger, R.K. McGuire, J.K. Mitchell, J.E. Shemeta, and J.L. Smith. 2012. *Induced Seismicity Potential in Energy Technologies*, 300. Washington, DC: The National Academies Press. ISBN:978-0-309-25367–3.

Horton, S. 2012. Disposal of hydrofracking waste water fluid by injection into subsurface aquifers triggers earthquake swarm in Central Arkansas with potential for damaging earthquake. *Seismological Research Letters* 83, no. 2: 250–260.

Hsieh, P.A., and J.D. Bredehoeft. 1981. A reservoir analysis of the Denver earthquakes: A case of induced seismicity. *Journal of Geophysical Research* 86, no. 2: 903–920.

Jaeger, C.J., and N.G.W. Cook. 1979. *Fundamentals of Rock Mechanics*. London: Methuen.

Kelkar, S., K. Lewis, S. Hickman, N. C. Davatzes, D. Moos, and G. Zyvoloski. 2012. Modeling coupled thermal-hydrological-mechanical processes during shear stimulation of an EGS well. In *Proceedings of Thirty-Seventh Workshop on Geothermal Reservoir Engineering*, Stanford University, Stanford, California, SGP-TR-194.

Kerr, R.A., and R. Stone. 2009. A human trigger for the great quake of Sichuan? *Science* 323: 322.

Lucier, A., M. Zoback, N. Gupta, and T.S. Ramakrishnan. 2006. Geomechanical aspects of CO_2 sequestration in a deep saline reservoir in the Ohio river valley region. *Environmental Geoscience* 13, no. 2: 85–103.

Manning, C.E., and S.E. Ingebritsen. 1999. Permeability of the continental crust: the implications of geothermal data and metamorphic systems. *Reviews of Geophysics* 37: 127–150.

Mark, C., and M. Gadde. 2008. Global trends in coal mine horizontal stress measurements. In *Proceedings 27th International Conference on Ground Control in Mining*, ed. S.S. Peng, S.C. Tadolini, C. Mark, G.L. Finfinger, K.A. Heasley, A.W. Khair, and Y. Luo, 319–331. Morgantown, WV: West Virginia University.

McBride, J.H., H.E. Leetaru, R.A. Bauer, B.E. Tingey, and S.E.A. Schmidt. 2007. Deep faulting and structural reactivation beneath the Southern Illinois Basin. *Precambrian Research* 15: 289–313.

Meremonte, M.E., J.C. Lahr, A.D. Frankel, J.W. Dewey, A.J. Crone, D.E. Overturf, D.L. Carver, and T.W. Bice. 2001. Investigation of an earthquake swarm near Trinidad, CO. USGS, Open-File Report 02–0073, Reston, Virginia: USGS.

Munson, P., S.F. Obermeier, C.A. Munson, and E. Hajic. 1997. Liquefaction evidence for Holocene and Latest Pleistocene seismicity in the southern halves of Indiana and Illinois: A preliminary overview. *Seismological Research Letters* 68, no. 4: 521–536.

Neuzil, C.E.. 2012. Hydromechanical effects of continental glaciation on groundwater systems. *Geofluids* 12: 22–37.

Nicholson, C., and R.L. Wesson. 1990. Earthquake hazard associated with deep well injection: a report to the U.S.

Environmental Protection Agency. U.S. Geol. Sur. Bull. 1951, Reston, Virginia: USGS.
Nicholson, C., E. Roeloffs, and R.L. Wesson. 1988. The Northeastern Ohio earthquakes of 31 january 1986: Was it induced? *Bulletin of the Seismological Society of America* 78, no. 1: 188–217.
O'Connell, D., and R. Creed. 2013. Determining injection-induced earthquake magnitude and ground motion exceedance probability using Paradox Valley, Colorado injection and seismicity data including paratmetric sensitivities. In *Proceeding of the Thirty-Eighth Workshop on Geothermal Reservoir Engineering*, SGP-TR-198.
Obermeier, S.F. 2009. Using liquefaction-induced features and other soft-sediment features for paleoseismic analysis. In *Paleoseismology*, 2nd ed., ed. J.P. McCaplin, 497–564. Amsterdam: Elsevier.
Obermeier, S.F., P.J. Munson, C.A. Munson, J.R. Martin, A.D. Frankel, T.L. Youd, and E.C. Pond. 1992. Liquefaction evidence for strong holocene earthquake(s) in the Wabash Valley of Indiana–Illinois. *Seismological Research Letters* 63: 321–335.
Olson, S.M., R.A. Green, and S.F. Obermeier. 2005. Revised magnitude-bound relation for the Wabash Valley seismic zone of the central United States. *Seismological Research Letters* 76, no. 6: 756–771.
Person, M., A. Banerjee, J. Rupp, C. Medina, P. Lichtner, C. Gable, R. Pawar, M. Celia, J. McIntosh, and V. Bense. 2010. Assessment of basin-scale hydrologic impacts of CO_2 sequestration, Illinois Basin. *International Journal of Greenhouse Gas Control* 4: 840–854.
Raleigh, C.B., J.H. Healy, and J.D. Bredehoeft. 1976. An experiment in earthquake control at Rangely, Colorado. *Science* 191: 1230–1237.
Raleigh, C.B., J.H. Healy, and J.D. Bredehoeft. 1972. Faulting and crustal stress at Rangely, Colorado. *American Geophysical Union Geophysical Monograph Series* 16: 275–284.
Reddy, J.N. 1984. *An Introduction to the Finite Element Method*. New York: McGraw Hill.
Rutqvist, J., J. Birkholzer, F. Cappa, and C.F. Tsang. 2007. Estimating maximum sustainable injection pressure during geological sequestration of CO_2 using coupled fluid flow and geomechanical fault-slip analysis. *Energy Conversion and Management* 48: 1798–1807.
Saar, M.O., and M. Manga. 2003. Seismicity induced by seasonal groundwater recharge at Mt. Hood, Oregon. *Earth and Planetary Science Letters* 214: 605–618.
Scholz, C.H. 2002. *The Mechanics of Earthquakes and Faulting*. Cambridge: Cambridge University Press.
Seeber, L., J.G. Armbruster, and W.Y. Kim. 2004. A fluid-injection-triggered earthquake sequence in Ashtabula, Ohio: implications for seismogenesis in stable continental regions. *Bulletin of the Seismological Society of America* 94, no. 1: 76–87.
Seeber, L., and J.G. Armbruster. 1993. Natural and induced seismicity in the Lake Erie-Lake Ontario region: reactivation of ancient faults with little neotectonic displacement. *Géographie physique et Quaternaire* 47, no. 3: 363–378.
Townend, J., and M.D. Zoback. 2000. How faulting keeps the crust strong. *Geology* 28: 399–402.
U.S. Environmental Protection Agency. 2010. Federal Requirements Under the Underground Injection Control (UIC) Program for Carbon Dioxide (CO_2) Geologic Sequestration (GS) Wells, *Federal Register*, 75. FR 77230. http://www.federalregister.gov/articles/2010/12/10/2010-29954/federal-requirements-under-the-undergroundinjection-control-uic-program-for-carbon-dioxide-co2#h-34.
Wheeler, R.L., and C.H. Cramer. 2002. Updated seismic hazard in the Southern Illinois Basin—Geological and geophysical foundations for use in the 2002 USGS national seismic hazard maps. *Seismological Research Letters* 73, no. 5: 776–791.
Zhang, Y., M. Person, C. Gable, J. Rupp, K. Ellett, K. Bandilla, T. Elliot, and M. Celia. 2011. Multi-layer, sharp-interface models of pore pressure buildup within the Illinois Basin due to basin-wide CO_2 injection. In *Paper Presented at the Annual AGU Fall Meeting* (Abstract), San Francisco, California, December 5–9.
Zhou, Q., J.T. Birkholzer, E. Mehnert, Y.F. Lin, and K. Zhang. 2010. Modeling basin- and plume-scale processes of CO_2 storage for full-scale deployment. *Ground Water* 48, no. 4: 494–514.
Zoback, M.D., and S.E. Gorelick. 2012. Earthquake triggering and large-scale geologic storage of carbon dioxide. *Proceedings of the National Academy of Sciences*. DOI:10.1073/pnas.1202473109.
Zoback, M.D., and J. Townend. 2001. Implications of hydrostatic pore pressures and high crustal strength for the deformation of intraplate lithosphere. *Tectonophysics* 336: 19–30.
Zoback, M.D., and H.P. Harjes. 1997. Injection-induced earthquakes and crustal stress at 9 km depth at the KTB deep drilling site, Germany. *Journal of Geophysical Research* 102, no. B8: 18477–18491.
Zoback, M.D., and M.L. Zoback. 1989. Tectonic stress field of the conterminous United States. *Geological Society of America Memoirs* 172: 523–539.